Anisotropy: Spin order and magnetization of single-crystalline Cu_{4}(OH)_{6}FBr barlowite

Tian-Heng Han, Eric D. Isaacs, John A. Schlueter, and John Singleton

Phys. Rev. B **93**, 214416 — Published 15 June 2016

DOI: 10.1103/PhysRevB.93.214416

Anisotropy: Spin Order and Magnetization of Single Crystalline $Cu_4(OH)_6FBr$

Tian-Heng Han[1,2†], Eric D. Isaacs[1], John A. Schlueter[2,3], and John Singleton[4]
[1] *James Frank Institute and Department of Physics, University of Chicago, Chicago, Illinois 60637, USA*
[2] *Materials Science Division, Argonne National Laboratory, Argonne, Illinois 60439, USA*
[3] *Division of Materials Research, National Science Foundation, Arlington, Virginia 22230, USA and*
[4] *National High Magnetic Field Laboratory, Los Alamos National Laboratory, Los Alamos, New Mexico 87545, USA*
(Dated: May 11, 2016)

Despite decades-long fascination, the difficulty of maintaining high lattice symmetry in frustrated non-bipartite $S = \frac{1}{2}$ materials that can also be made into high-quality single crystals has been a persistent challenge. Here we report magnetization studies of a single-crystal sample of barlowite, $Cu_4(OH)_6FBr$, which has a geometrically perfect kagome motif. At $T \leq 4.2$ K and $35 \leq \mu_0 H \leq 65$ T, the interlayer spins are fully polarized, and the kagome-intrinsic magnetization is consistent with a Heisenberg model having $J/k_B = -180$ K. Several field-driven anomalies are observed, having varies scalings with temperature. At an applied field, kagome disorder caused by the interlayer spins is smaller than that in herbertsmithite. At $T \leq 15$ K, the bulk magnetic moment comes from the interlayer spins. An almost coplanar spin order suggests that the magnitude of in-plane Dzyaloshinskii-Moriya interaction is smaller than 0.006(6) J. On the other hand, the possibility of a spin-liquid state in the kagome lattice coexisting with ordered interlayer spins is left open.

PACS numbers: 75.30.Gw, 75.30.Cr, 75.50Ee, 75.10.Jm

Quantum magnets, materials containing spins with strong correlations, often exhibit counterintuitive behavior, in which quantum mechanics is writ large[1–3]. The effect of quantum fluctuations is strong in the presence of frustration, prohibiting simple forms of magnetic order, such as ferro- and antiferromagnetism. When the magnetic ground state features a large entanglement of spins, a quantum spin liquid (QSL) can be realized—a magnet without any ordered or frozen moments, even at temperature $T = 0$, despite the presence of strong interactions[1]. In most frustrated quantum magnets, spin-rotational symmetry is broken at low temperatures, offering a variety of unconventional orders, such as spin-density waves, spin-nematic phases[3], magnetization-plateau states[4] and topological magnons[5].

Antiferromagnetic interactions on a triangular plaquette prohibit the satisfaction of all exchange interactions and thus frustrate conventional forms of spin order. κ-(BEDT-TTF)$_2$Cu$_2$(CN)$_3$ and EtMe$_3$Sb[Pd(dmit)$_2$]$_2$ are two QSL candidates featuring slightly distorted triangular lattices of $S = \frac{1}{2}$ molecular pairs[1]. However, the rapidly-diminishing magnetic form factor due to the diffuse electrons[6], the low spin density, and the thinness of the crystals prohibits decisive experiments. Transition metal ions provide $S = \frac{1}{2}$ entities that do not suffer from these problems[7]. In triangular and kagome compounds of small-spin $3d$ ions, the Jahn-Teller effect distorts the geometry of almost all candidate compounds. Herbertsmithite remains the only $S = \frac{1}{2}$ antiferromagnet with an undistorted kagome motif for which large single crystals are available[8–10], although local structural distortions may exist[11]. In addition, its nonstoichiometric disorder and elusive spin Hamiltonian complicate the interpretation of experimental observations[12–14].

The recent synthesis of barlowite, $Cu_4(OH)_6FBr$, provides new and fascinating opportunities. Barlowite crystallizes in the space group $P6_3/mmc$. Three quarters of the Cu^{2+} ions form a direct stack of undistorted kagome lattices with the remaining Cu^{2+} ions occupying interlayer sites. The Curie-Weiss temperature $\approx 136(10)$ K[15] reflects mostly a uniform kagome exchange, which is antiferromagnetic[16]. Below 15 K, a weak ferromagnetic moment, likely an effect of the interlayer spins, appears in polycrystalline samples. Barlowite's high crystallographic symmetry and exciting thermodynamic properties attracted immediate attention from the theoretical community[16–18]. In this Letter, we present magnetic measurements on a high-quality single-crystal sample of barlowite that show that it is a model system for exploring spin order on an undistorted spin-$\frac{1}{2}$ kagome antiferromagnet.

Figure 1(a) shows magnetization of a 5.4 mg single crystal of barlowite, measured as a function of temperature using a SQUID magnetometer (Quantum Design MPMS). The nearly cubic shape of the sample minimizes demagnetization anisotropy, allowing for an accurate determination of the intrinsic magnetic anisotropy. The crystal was attached to the inner surface of a uniform plastic straw using Aperizon N grease weighing < 0.1 mg. The background from the grease was measured to be negligible. For $\mathbf{H} \perp \mathbf{C}$ (where the $\mathbf{C}$ axis is normal to the kagome lattice) the magnetization ($M_\perp$) measured after cooling in a 0.005 T field indicates a weak ferromagnetic transition at 15.4 K, in agreement with measurements on a polycrystalline sample[15]. The zero-field-cooled (ZFC) magnetization deviates from that measured under field-cooled (FC) conditions, exhibiting thermal hysteresis. Owing to the remanent field (≈ 1 mT) of the superconducting magnet,

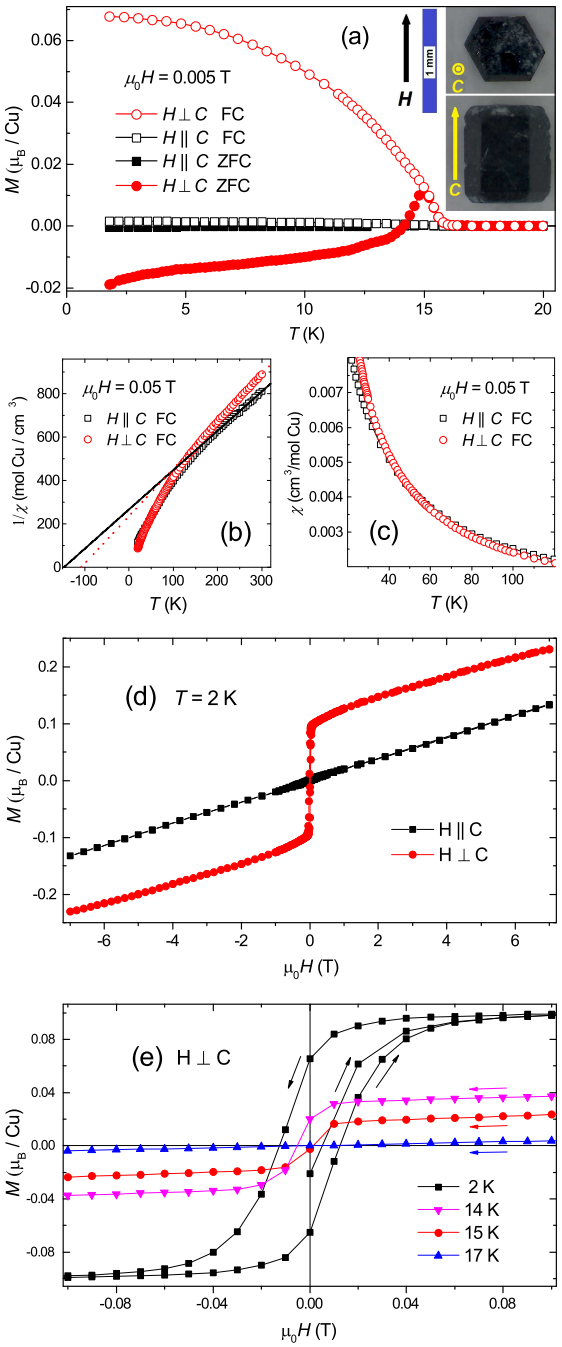

FIG. 1: (a) Magnetization of a single-crystal of barlowite measured in a field of 5 mT applied normal (**H**||**C**) or parallel (**H** ⊥ **C**) to the kagome lattice after zero-field cooling (ZFC) and field cooling (FC). Inset: A single crystal of barlowite viewed along the **C**-axis (top) and the kagome lattice plane (bottom). (b) Inverse susceptibility and Curie-Weiss fits at 0.05 T. (c) Susceptibility at 0.05 T. (d) Anisotropic magnetization at 2 K. (e) Hysteresis loop for **H** ⊥ **C**.

the ZFC magnetization is slightly negative at low temperatures. Because 0.005 T is lower than the coercive field[15], the ZFC curve only becomes positive when the temperature approaches 15 K. For **H**||**C**, both ZFC and FC curves ($M_{||}$) are close to zero.

The inverse susceptibility ($1/\chi$) measured at 0.05 T is shown in Fig. 1(b). For these measurements, the sample has been rotated *in situ* by deforming the plastic straw in order to preserve the identical, although very small, background. Curie-Weiss fits have been performed for $T \geq 180$ K. Using mean-field analysis, we determine Curie-Weiss temperatures and g factors $\Theta_{\mathrm{CW}||} = -147(10)$ K and $g_{||} = 2.42(5)$ for **H**||**C** and $\Theta_{\mathrm{CW}\perp} = -108(10)$ K and $g_\perp = 2.21(5)$ for **H** ⊥ **C**. Fig. 1(c) shows that $\chi_{||} < \chi_\perp$ below 50 K, where the χ are measured parallel and perpendicular to the **C** axis respectively; conversely, $\chi_{||} > \chi_\perp$ above 50 K.

Low-field $M(H)$ measurements were made using the SQUID magnetometer. In Fig. 1(d), the $M(H)$ loop at 2 K is shown for field sequence $0 - +7$ T $- -7$ T $- +7$ T. For $\mu_0 H < 0.1$ T, $M_\perp$ exhibits a hysteresis loop while $M_{||}$ shows almost none. Panel (e) zooms into the hysteresis loop at $T = 2$ K for **H** ⊥ **C**. The remanent magnetization is $M_{\mathrm{r}\perp} = 0.065 \pm 0.001 \mu_{\mathrm{B}}$/Cu and the coercive field is $\mu_0 H_{\mathrm{c}\perp} = 13 \pm 1$ mT. Upon warming above 15 K, both the remanence and coercivity vanish. A similar zooming for **H**||**C** reveals a much smaller remanent magnetization, $M_{\mathrm{r}||} = 0.0023 \pm 0.0001 \mu_{\mathrm{B}}$/Cu.

The very small value of $M_{\mathrm{r}||}$ indicates that the spin order in barlowite is almost coplanar, which is also supported by the anisotropy seen in Fig. 1(a). Nearest-neighbor exchange interactions are equal in the kagome lattice[16]. Taking the perturbations from the interlayer spins into consideration[15] and assuming all spins order below 15 K, the kagome spins likely settle into an almost 120-degree pattern[19] with interlayer spins aligning to adjacent kagome spins. $M_{\mathrm{r}||}$ may come from a projection of $M_{\mathrm{r}\perp}$ and/or a minimum intrinsic ordered moment perpendicular to the kagome lattice. Assuming a perfect alignment of the crystal in the field, the maximum out-of-plane spin canting angle η can be estimated. In Fig. 3(a) (see discussion below), no spin flip is observed, thus the kagome spins likely cant towards the same direction along the **C**-axis. This gives $\eta \leq 0.2(2)^\circ$, taking the uncertain sizes of the ordered moments into consideration. The lattice symmetry of barlowite permits the Dzyaloshinskii-Moriya interaction (DMI). The out-of-plane component of the DMI provides an effective easy-plane anisotropy; the in-plane component gives an effective easy-axis anisotropy[20]. The vanishing $M_{\mathrm{r}||}$ suggests that the magnitude of in-plane DMI is smaller than 0.006(6) J[20].

Figure 2 shows the same data as Figure 1 (b) and (c) do. The data for **H** ⊥ **C** is corrected with g-factor ratio. At $T > 100$ K, the intrinsic isotropy of the kagome spins unveils, bearing out a Heisenberg spin model. When cooling below 100 K, anisotropy gradually builds up from the quickly increasing anisotropic magnetization of the interlayer spins.

Figure 3 shows magnetization $M(H)$ measured using an extraction magnetometer, in a ^{3}He cryostat, in fields of up to 65 T, provided by a 100-ms-duration

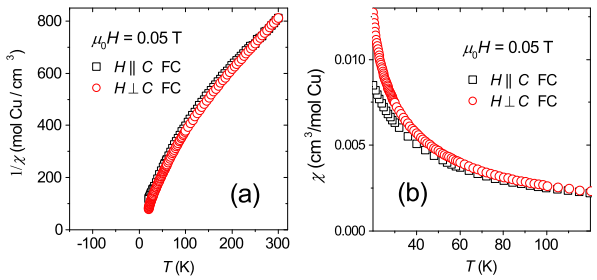

FIG. 2: Inverse susceptibility (a)/susceptibility (b) at 0.05 T as shown in Figure 1(b)/(c) but with g-factor corrections. The inverse susceptibility/susceptibility for $\mathbf{H} \perp \mathbf{C}$ is divided/multiplied by $g_{||}/g_{\perp}$=2.42/2.21.

pulsed magnet at the National High Magnetic Field Laboratory in Los Alamos[21]. The magnetometer was calibrated against SQUID measurements. Several single crystals were carefully coaligned for measurements in each field orientation. Great care was taken to ensure that the crystals did not move or rotate in the field. $M(H)$ has been normalized to the saturation moment by assuming $S = \frac{1}{2}$ for Cu^{2+} ions and taking the g factor into consideration. For $T \leq 4.2$ K, $M(H)$ is temperature independent, and the curve shown in panel (a) is an average of data taken at several temperatures. No hysteresis is observed for $\mathbf{H}||\mathbf{C}$, consistent with Fig. 1(d).

The absence of hysteresis for $\mathbf{H}||\mathbf{C}$ contradicts ref.16, which reports a large hysteresis with a virgin curve falling outside the loop. The latter data can be explained by initial imperfect alignment of the crystal in the field followed by a magnetic-torque driven rotation, accounting for the upward bending of the virgin curve beyond 1 T seen in ref. 16. As shown in Fig. 1(d), the easy axis of magnetization is perpendicular to $\mathbf{C}$. This is consistent with the direction of the crystal rotation. Moreover, in ref. 16, $M(H)$ for $\mathbf{H}||\mathbf{C}$ quantitatively matches our measurements for $\mathbf{H} \perp \mathbf{C}$ presented in Fig. 1(e). Our hypothesis also explains a large magnetization at $T < 15$ K for $\mathbf{H}||\mathbf{C}$ reported in ref.16, which contradicts the result in Fig. 1(a).

In all measurements shown in Fig. 3, the slope of $M(H)$ versus H decreases after a few tesla. For $\mathbf{H}||\mathbf{C}$, the field gradually polarizes the interlayer spins while canting the kagome spins. At $T = 5$ K, Fig. 3(a) and its inset show that a *high-field* feature in $\mathrm{d}M_{||}/\mathrm{d}H$ appears at about 30 T, beyond which $\mathrm{d}M_{||}/\mathrm{d}H$ drops to a constant. This feature progressively fades out as T increases, and is absent for $\mathbf{H} \perp \mathbf{C}$. For $T \leq 4.2$ K, the zero-field intercept of a linear fit to the data above 45 T is $0.29(1)\mu_{\mathrm{B}}$ per Cu. This value is consistent with a full polarization of the interlayer spins that also weakly polarizes the kagome spins. The slope of the fit is 0.00202(10)/T, giving an estimated saturation field of 350 ± 20 T. For a kagome antiferromagnet, saturation occurs at $\mu_{\mathrm{B}}B = 3J$. For $S = \frac{1}{2}$ and $g = 2.3$, 350 T is consistent with $J/k_{\mathrm{B}} = -180$ K[15]. For $\mathbf{H} \perp \mathbf{C}$, $\mathrm{d}M_{\perp}/\mathrm{d}H$

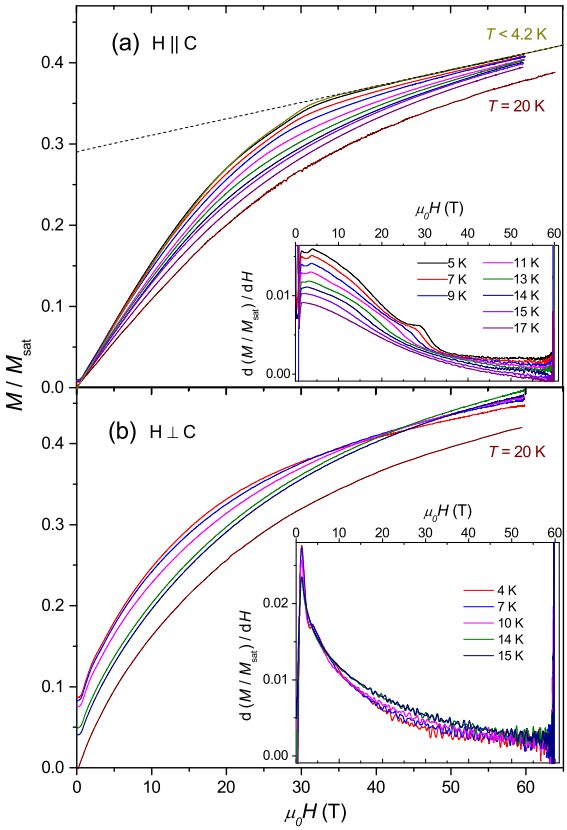

FIG. 3: Magnetization vs field applied normal (a) or parallel (b) to the kagome lattice, for temperatures from $T \leq 4.2$ K to $T = 20$ K. M_{sat} represents the saturation moment for each configuration. Insets: $\mathrm{d}M/\mathrm{d}H$ vs H at selected temperatures. For the inset in panel (a), the data at 7 K are offset by -0.00049 along the vertical axis from the original value. For $T > 7$ K, the data are offset by an additional -0.00049 for each successively higher temperature.

decreases gradually as the field increases, making an accurate determination of the field beyond which the interlayer spins are fully polarized for this orientation difficult. Nevertheless, a linear fit to the data for $50 \leq \mu_0 H \leq 57$ T gives a slope of 0.00199(10)/T. This equals the value for $\mathbf{H}||\mathbf{C}$ within the errors, consistent with the prior suggestion of a Heisenberg model. For $T \leq 15$ K, a small magnetization appears at zero field, and so does anisotropy.

Figure 4 exhibits $\mathrm{d}M/\mathrm{d}H$ at $\mu_0 H < 5$ T in greater detail. At $T = 4$ K for each field orientation, a *low-field* anomaly appears at 3.8 T. As T rises, the peak moves to lower fields, and eventually disappears above 15 K.

In the inset of Fig. 3(a), $\mathrm{d}M_{||}/\mathrm{d}H$ data are fitted to function $a[\cosh(bT)]^{-2} + A\exp[(T-B)^2/D^2]$, where the first term is the derivative of the spin$-\frac{1}{2}$ Brillouin function, the second term models a Gaussian peak, and a, b, A, B and D are constants. Values of B, the position of the *high-field* anomaly, are plotted as a function of T in Fig. 5(a) and fitted to a power law $M = \kappa(15.4 - T)^{\beta_{\mathrm{hf}}}$ for $8 \leq T \leq 14$ K, where κ is a constant. The critical exponent $\beta_{\mathrm{hf}} = 0.50(4)$, iden-

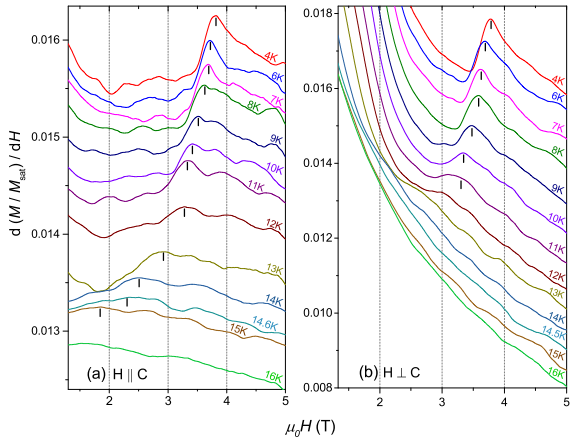

FIG. 4: $\mathrm{d}M/\mathrm{d}H$ vs H applied normal (a) or parallel (b) to the kagome lattice. The ticks are guides for the eye in following peak positions. In (b) at $T = 6\ K$, the data are offset by -0.00065 along the vertical axis from the original value. For $T > 6\ K$, the data are offset by an additional -0.00065 at each successively higher temperature.

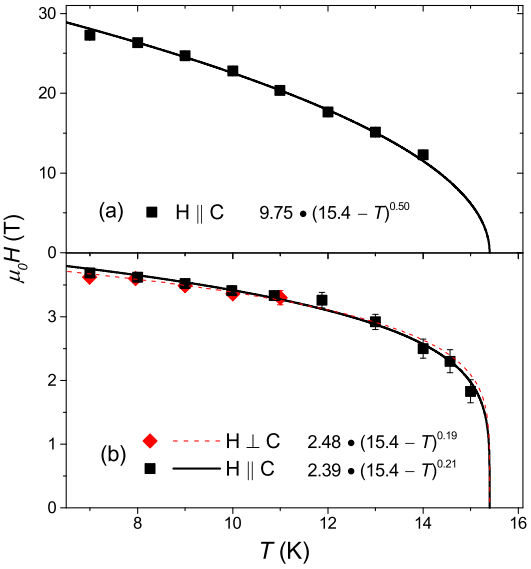

FIG. 5: Temperature scalings of field-driven anomalies presented in Fig. 3(a) inset, panel a, and in Fig. 4, panel b. Power-law fits are shown.

tical, within errors, to that for the temperature dependence of the magnetization $M(T)$ at almost zero field, $\beta_T = 0.51$[15]. In Fig. 5(b), temperature scalings of the *low-field* anomalies (shown in Fig. 4) are plotted and fitted to the same functional form, giving $\beta_{lf||} = 0.21(3)$ for $\mathbf{H}||\mathbf{C}$ and $\beta_{lf\perp} = 0.19(3)$ for $\mathbf{H} \perp \mathbf{C}$.

When cooling below 50 K, as shown in Fig. 1(c), the switch from easy-axis to easy-plane magnetization anisotropy qualitatively resembles measurements on herbertsmithite[22], in which anisotropic interlayer magnetization dominates below the switching temperature. Moreover, the magnetic entropy of barlowite below the spin ordering temperature shifts to higher temperatures at applied fields of only a few tesla[15]; this is also similar to the behavior of interlayer spins in herbertsmithite[22], These observations suggest that the measured spin order in barlowite comes mostly from the interlayer physics, and provide a hint as to why $\beta_{\mathrm{hf}} \approx \beta_T$. $\beta_{\mathrm{lf}||}$ and $\beta_{\mathrm{lf}\perp}$ deviate significantly from β_{hf}, indicating that the *low-field* anomalies might come from the kagome spins. The fact that $\beta_{\mathrm{lf}||} \approx \beta_{\mathrm{lf}\perp}$ is consistent with Heisenberg exchange within the kagome lattice[16]. It is worth noting that $\beta_{\mathrm{lf}||}$ and $\beta_{\mathrm{lf}\perp}$ are close to those obtained in the $S = \frac{5}{2}$ kagome antiferromagnet $KFe_3(OH)_6(SO_4)_2$, which undergoes spin flips in an applied field[23].

Figure 6(a) zooms below 1 tesla for $\mathbf{H}||\mathbf{C}$, revealing two more anomalies. For $6 \leq T \leq 13$ K, two subtle peaks occur at 0.42(2) T and 0.87(3) T. When warming to 14 K, which is between two phase transitions at 13.8 K and 15.4 K [15], the 0.87 T peak diminishes while the 0.42 T peak gets stronger before it gradually fades out for $T > 15$ K. Interestingly, the 0.87 T peak shifts down to 0.71 T for $T \leq 4$ K (lower temperatures not shown). By contrast, in Fig. 6(b) a broad hump extends from 0.5 T to 2.5 T at $T = 4$ K for $\mathbf{H} \perp \mathbf{C}$. On warming, as shown in Fig.6(c), the hump flattens and eventually disappears for $T \geq 15$ K. Several weak transitions are expected, given the complexity of the competing interactions and their energy scales[16], but it is beyond the scope of the present paper to say exactly what they are; this would demand a much more intensive theoretical effort, hopefully, stimulated by our experimental characterization.

A recent density functional theory (DFT) calculation gives a kagome antiferromagnetic exchange of $J_{\mathrm{DFT}} = -177$ K[16]. The exchange interactions between an interlayer Cu and the six adjacent kagome spins are all ferromagnetic, including two strong $J'_{1\mathrm{DFT}}$'s of 205 K and four weak $J'_{2\mathrm{DFT}}$'s of 32 K. The average of the six exchange energies is $J'_{\mathrm{DFT}} = 90$ K $\approx -\frac{J}{2}$, at odds with the analysis of polycrystalline magnetization[15]. In Fig. 7(a), χT is calculated from the susceptibility measured on the single-crystal sample at 0.05 T and compared with various calculations. The numerical linked-cluster expansion (NLCE) and exact diagonalization (ED) methods[24] assumed $g = 2.3$ and a weak ferromagnetic $J' = -0.1J$ between an interlayer Cu and the kagome spins. Because of the finite-lattice effect, the precision of NCLE and ED decreases at low temperatures, especially when $T < 0.2J/k_{\mathrm{B}}$. The series expansion (SE)[16] assumed parameters close to those of the DFT calculation and was scaled to match data at high temperatures. The NCLE and ED curves follow the data much more closely than does the SE curve. As temperature decreases, the SE curve increases faster than the data and turns up quickly at a temperature much higher than the ordering temperature. This suggests that J'_{DFT} used in the SE

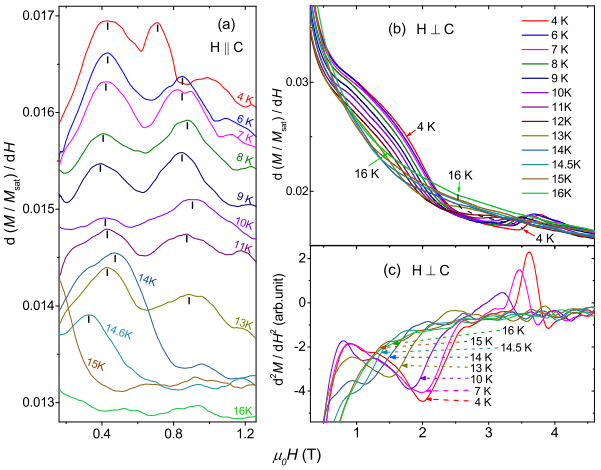

FIG. 6: $\mathrm{d}M/\mathrm{d}H$ vs H applied normal (a) or parallel (b) to the kagome lattice. (a) The ticks guide the eye in following peak positions. (b) Along the dashed line, T varies from 16 to 4 K. $\mathrm{d}M^2/\mathrm{d}H^2$ at selected temperatures for panel (b).

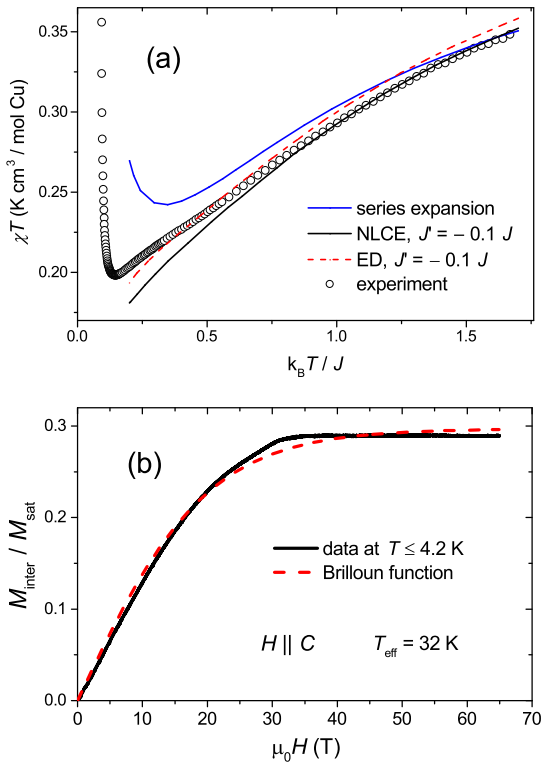

FIG. 7: (a) Comparison of a polycrystalline-average susceptibility (calculated from the single-crystal data shown in Fig. 1(b)) with theories in the presence of a ferromagnetic out-of-kagome-plane exchange. The x-axis is normalized to $J/k_{\mathrm{B}} = -180$ K[15]. (b) Polarization of the interlayer spins is fitted using a Brillouin function for **H**||**C**.

calculation is too large.

The interlayer magnetization at $T \leq 4.2$ K is obtained by subtracting the high-field kagome-intrinsic contribution, as shown in Fig. 7(b). The M_{inter} vs H curve is fitted with a spin$-\frac{1}{2}$ Brillouin function, by using the effective temperature T_{eff} as a free parameter. T_{eff} is an estimate of the effective interaction on an interlayer spin. The returned value, $T_{\mathrm{eff}} = 32$ K for **H**||**C**, is much larger than the measurement temperature and thus represent the average J' between an interlayer spin and a kagome spin. The small excess magnetization, 16% of the value permitted for stoichiometric composition, is another indication of a small J'.

In applied fields, the impurity magnetization of herbertsmithite is approximately twice that permitted for the interlayer spins[25], which likely polarize the kagome lattice through superexchange and thus induce intra-kagome disorder[26]. The interlayer spins affect about half of the kagome lattice[25] and efforts to chemically minimize their concentration have been unsuccessful. Recent neutron scattering[11] and nuclear magnetic resonance[27] experiments show evidence that, at zero applied field, the kagome lattice of herbertsmithite has a spin gap while the interlayer spins are separately modeled as a correlated cluster. Without a field, the kagome lattice is largely immune from disorder, because most of the interlayer spins dangle[11]. On the other hand, no spin ordering occurs at fields large enough to close the spin gap, nor does the appearance of a Zeeman gap[28,29]. This suggests that, in applied fields, the interlayer moments cannot be separated from the kagome spins in a trivial manner. When establishing a complete phase diagram connecting the zero-field ground state and its in-field variations, this conundrum complicates the interpretation of herbertsmithite's properties[26]. By contrast, in barlowite, the excess magnetization is 16% of the value permitted for stoichiometric composition. The different scalings in Fig. 5, the small $J' \sim -0.1J$[15], and the small excess magnetization implies that the kagome layers of barlowite are only weakly perturbed by the interlayer spins. Future quantification of the perturbative exchanges may be extracted from single-crystal spin-wave analysis using inelastic neutron scattering.

Spin-liquid physics is not precluded by small ordered moments[2,30]. In Cs_2CuCl_4, a spinon continuum has been observed despite an ordered ground state[31]. It is worth seeking similar phenomena in barlowite, given that the entropy release at phase transitions is less than 20% of the total expected value[15]. The measurements can be performed at a temperature above the ordering transition, and as such, the consequence of perturbations is reduced. The spin-liquid dynamics likely survives to $T = 100$ K, as is the case in herbertsmithite[14]. More exotically, the kagome spins may form a spin liquid while the interlayer spins order below 15 K. In this scenario, the interlayer spins polarize the dynamic kagome moments, which meditate the exchanges among interlayer spins. This hypothesis explains the missing spin entropy, and is consistent with the absence of spin canting. It is also theoretically plausi-

ble since spin-liquid states can be stable to perturbations $\sim 0.1J$ in size[2]. The evidence of a spin gap in herbertsmithite suggests a robust spin-liquid state in the presence of perturbations and disorder[11,27]. In barlowite, interlayer spins project out-of-kagome perturbations while kagome site disorder is absent. Whether a spin-liquid state survives the ordering is an open question.

The DMI in herbertsmithite is similar[32] to the very small in-plane DMI in barlowite, whilst that in vesignieite is an order of magnitude larger; in the latter, a relatively high spin-ordering temperature results[33]. As opposed to herbertsmithite with its staggered kagome stacking, barlowite crystalises in high-symmetry hexagonal rods owing to direct kagome stacking. This is an important advantage in our magnetometry measurements, because it allows precise orientation and minimization of the background. Barlowite crystals are cleavable in the kagome plane [001][34], making surface-sensitive techniques (ARPES, STM, etc) potentially feasible. A finite conductivity is observed from optical measurements due to spin-charge interactions[35]. In kagome antiferromagnets, non-trivial spin orders have been studied on large-spin compounds using single crystals and on small-spin materials using polycrystalline samples. Barlowite finally provides the long-sought playground for spin order on an undistorted spin-$\frac{1}{2}$ kagome antiferromagnet that is available as single crystals.

In summary, barlowite exhibits magnetic properties consistent with a Heisenberg kagome antiferromagnet with weak interlayer spin coupling. Its almost coplanar spin order and multiple field-driven features in magnetization motivate further studies. In addition to its promise for new spin-liquid states, barlowite appears to host intriguing spin textures of its own.

We thank Patrick Lee, David Huse, Yasu Takano and Thomas Rosenbaum for careful reading with useful comments. T.-H. H. acknowledges the support of the Grainger Fellowship provided by the Department of Physics, University of Chicago and the support from the Department of Energy (DOE) (DE-FG02-99ER45789, DE-AC02-06CH11357). J. A. S. acknowledges support from the NSF Independent Research/Development program. A portion of this work was performed at the National High Magnetic Field Laboratory, which is supported by NSF Cooperative Agreement No. DMR-1157490, the State of Florida, the DOE and through the DOE Basic Energy Science Field Work Proposal "Science in 100 T".

†tianheng@alum.mit.edu

[1] L. Balents, Nature **464**, 199 (2010).
[2] L. Savary and L. Balents, arXiv:1601.03742 (2016).
[3] O. A. Starykh, Rev. Prog. Phys. **78**, 052502 (2015).
[4] H. Ishikawa, M. Yoshida, K. Nawa, M. Jeong, S. Krämer, M. Horvatić, C. Berthier, M. Takigawa, M. Akaki, A. Miyake, et al., Phys. Rev. Lett. **114**, 227202 (2015).
[5] M. Hirschberger, R. Chisnell, Y. S. Lee, and N. P. Ong, Phys. Rev. Lett. **115**, 106603 (2015).
[6] F. Salvat-Pujol, H. O. Jeschke, and R. Valentí, Phys. Rev. B **90**, 041101 (2014).
[7] T. M. McQueen, T. H. Han, D. E. Freedman, P. W. Stephens, Y. S. Lee, and D. G. Nocera, J. Solid State Chem. **184**, 3319 (2011).
[8] T. H. Han, J. S. Helton, S. Chu, A. Prodi, D. K. Singh, C. Mazzoli, P. Müller, D. G. Nocera, and Y. S. Lee, Phys. Rev. B **83**, 100402R (2011).
[9] D.Wulferding, P.Lemmens, P.Scheib, J.Röder, P.Mendels, S.Chu, T.Han, and Y.S.Lee, Phys. Rev. B **82**, 144412 (2010).
[10] M. R. Norman, arXiv:1606.03048 (2016).
[11] T.-H. Han, M. R. Michael, J.-J. Wen, J. A. Rodriguez-Rivera, J. S. Helton, C. Broholm, and Y. S. Lee, arXiv:1512.06807 (2015).
[12] D. E. Freedman, T. H. Han, A. Prodi, P. Müller, Q. Z. Huang, Y. S. Chen, S. M. Webb, Y. S. Lee, T. M. McQueen, and D. G. Nocera, J. Am. Chem. Soc. **132**, 16185 (2010).
[13] O. Ofer, A. Keren, J. H. Brewer, T. H. Han, and Y. S. Lee, J. Phys. Condens. Matter. **23**, 164207 (2011).
[14] T.-H. Han, J. S. Helton, S. Chu, D. G. Nocera, J. A. Rodrigues-Rivera, C. Broholm, and Y. S. Lee, Nature **492**, 406 (2012).
[15] T.-H. Han, J. Singleton, and J. A. Schlueter, Phys. Rev. Lett. **113**, 227203 (2014).
[16] H. O. Jeschke, F. Salvat-Pujol, E. Gati, N. H. Hoang, B. Wolf, M. Lang, J. A. Schlueter, and R. Valentí, Phys. Rev. B **92**, 094417 (2015).
[17] Z. Liu, X. Zou, J.-W. Mei, and F. Liu, Phys. Rev. B **92**, 220102R (2015).
[18] D. Guterding, H. O. Jeschke, and R. Valentí, arXiv:1511.05686 (2015).
[19] M. J. Lawler, L. Fritz, Y. B. Kim, and S. Sachdev, Phys. Rev. Lett. **100**, 187201 (2008).
[20] M. Elhajal, B. Canals, and C. Lacroix, Phys. Rev. B **66**, 014422 (2002).
[21] P. A. Goddard, T. Lancaster, S. J. Blundell, J. Singleton, P. Sengupta, R. D. McDonald, S. Cox, N. Harrison, F. L. Pratt, J. L. Manson, H. I. Southerland, and J. A. Schlueter, New J. Phys. **10**, 083025 (2008).
[22] T. Han, S. Chu, and Y. S. Lee, Phys. Rev. Lett. **108**, 157202 (2012).
[23] D. Grohol, K. Matan, J.-H. Cho, S.-H. Lee, J. W. Lynn, D. G. Nocera, and Y. S. Lee, Nat. Mater. **4**, 323 (2005).
[24] E. Khatami, J. S. Helton, and M. Rigol, Phys. Rev. B **85**, 064401 (2012).
[25] T. Imai, M. Fu, T. H. Han, and Y. S. Lee, Phys. Rev. B **84**, 020411R (2011).
[26] T. Shimokawa, K. Watanabe, and H. Kawamura, Phys. Rev. B **92**, 134407 (2015).
[27] M. Fu, T. Imai, T.-H. Han, and Y. S. Lee, Science

350, 655 (2015).
[28] T.-H. Han, R. Chisnell, C. J. Bonnoit, D. E. Freedman, V. S. Zapf, N. Harrison, D. G. Nocera, Y. Takano, and Y. S. Lee, arXiv:1402.2693 (2014).
[29] T. Asaba, T.-H. Han, B. J. Lawson, F. Yu, C. Tinsman, Z. Xiang, G. Li, Y. S. Lee, and L. Li, Phys. Rev. B **90**, 064417 (2014).
[30] L. D. C. Jaubert, SPIN **05**, 1540005 (2015).
[31] R. Coldea, D. A. Tennant, A. M. Tsvelik, and Z. Tylczynski, Phys. Rev. Lett. **86**, 1335 (2001).
[32] A. Zorko, S. Nellutla, J. van Tol, L. C. Brunel, F. Bert, F. Duc, J. C. Trombe, M. A. de Vries, A. M. Harrison, and P. Mendels, Phys. Rev. Lett. **101**, 026405 (2008).
[33] A. Zorko, F. Bert, A. Ozarowski, J. van Tol, D. Boldrin, A. S. Wills, and P. Mendels, Phys. Rev. B **88**, 144419 (2013).
[34] P. Elliott, M. A. Cooper, and A. Pring, Min. Mag. **78**, 1755 (2014).
[35] D. V. Pilon, C. H. Lui, T.-H. Han, D. Shrekenhamer, A. J. Frenzel, W. J. Padilla, Y. S. Lee, and N. Gedik, Phys. Rev. Lett. **111**, 127401 (2013).